journal

J. Am. Ceram. Soc., 80 [12] 3029–37 (1997)

# Delamination Resistance of Two Hybrid Ceramic-Composite Laminates

Willard A. Cutler,*,† Frank W. Zok,* and Fred F. Lange*

Materials Department, University of California, Santa Barbara, California 93106

Panos G. Charalambides*

Department of Mechanical Engineering, The University of Maryland–Baltimore County, Baltimore, Maryland 21228

**Hybrid laminar composites that are comprised of alternating layers of ceramic sheets and fiber-reinforced ceramic-matrix composite (CMC) layers exhibit attractive mechanical properties, including a high first cracking stress and a high strain to failure. To achieve these properties, a strong bond must exist between the ceramic and CMC layers; otherwise, delamination will occur readily between the layers. The present study focuses on the delamination resistance of such laminates at ambient and elevated temperatures. The delamination resistance of interfaces that have been subjected to mixed-mode loading has been measured for two different hybrid composites by using edge-notched flexure specimens. At low temperatures, delamination occurs by a process that involves multiple matrix cracking within the CMC layers normal to the fibers, followed by cracking of the matrix parallel to the fibers at or near the ceramic/CMC interface. The corresponding fracture energies are typically in the range of ~100–300 J/m$^2$—comparable to the delamination resistance of the CMC itself. At elevated temperatures, delamination occurs via cavitation and rupture of the matrix within the CMC layers at or near the ceramic/CMC interface, with an attendant loss in toughness (to ~10–30 J/m$^2$). The loss in toughness occurs most rapidly at temperatures that are close to the strain point of the matrix phase; this represents the life-limiting temperature for this class of composites.**

## I. Introduction

HYBRID laminar composites are fabricated by bonding together alternating layers of a monolithic ceramic and a fiber-reinforced ceramic-matrix composite (CMC) at elevated temperatures, using the matrix phase of the CMC as the bonding agent. A variety of such composites have previously been fabricated and their properties have been characterized.[1,2] A distinct advantage of this compositing scheme over conventional fiber CMCs is that the constituent layers can be first fabricated independently of each other, following a route that optimizes their respective mechanical properties. Subsequently, the layers can be selected and combined in such a way that the ceramic layers impart a high cracking stress (provided that they are stiff and strong) and the CMC layers provide a high strain to failure and good damage tolerance. This processing route can provide considerable flexibility and tailorability in mechanical properties.

To obtain good structural properties in the hybrid laminates, the layers must be strongly bonded to each other. Laminates with weak interfaces are susceptible to delamination under out-of-plane tensile loading. Under in-plane loading, delamination may also occur, as a result of cracks that form in the monolithic ceramic layers perpendicular to the interfaces and deflect into the interfaces. Such effects are important both in uniaxial tension and in bending. The problem of delamination in weakly bonded systems can be exacerbated in bend tests that are performed on relatively short beams, wherein the shear stresses between the outer and inner loading pins can precipitate shear delamination prior to tensile cracking of the layers. When delamination occurs, the layers bend essentially independently of each other, and each has a linear stress gradient, from tension to compression (provided that the frictional resistance is small). The subsequent tensile failure occurs at a significantly lower load level. Such effects have been demonstrated at ambient temperatures in several different laminates[1–3] and are expected to be equally important at elevated temperatures.

Recent studies have demonstrated the importance of delamination in controlling both the flexural and tensile properties of these laminates.[2,3] At sufficiently high temperatures, their mechanical properties rapidly degrade. This degradation is manifested in the development of extensive delamination along or near the ceramic/CMC interfaces. Evidently, the delamination resistance is strongly temperature dependent. The purpose of the present study is to experimentally examine the temperature dependence of the delamination resistance of two different ceramic/CMC laminates and, in particular, to identify the critical temperature at which the degradation is most acute. It is demonstrated that the delamination resistance steeply decreases at temperatures that roughly correspond to the strain point[‡] of the matrix material within the CMC layers of these laminates.

## II. Experimental Procedure

Two different hybrid laminates were studied. Both were fabricated with dense SiC sheets that were ~0.5 mm thick (Hexoloy SA, Carborundum Co., Niagara Falls, NY). The CMC layers[§] were comprised of either Nicalon™ SiC fibers (Nippon Carbon, Tokyo, Japan) within a glass matrix (aluminosilicate glass, Corning 1723, Corning, NY) or of Nicalon fibers in a glass-ceramic matrix (calcium aluminosilicate glass-ceramic, Corning-CAS, Corning). Table I lists the strain, annealing, and

B. N. Cox—contributing editor

Manuscript No. 191281. Received January 13, 1997; approved April 22, 1997.
Supported in part by the DARPA University Research Initiative Program at UCSB under Office of Naval Research Contract No. N00014-92-J-1808. Author WAC was supported by Corning (Corning, NY). Author PGC was supported by the National Science Foundation under Grant No. CMS 94-96209.

*Member, American Ceramic Society.
†Now with Corning, Corning, NY.

‡Usually, the key changes in the flow characteristics of glasses are characterized by the strain point, the annealing point, and the softening point; these correspond to viscosities of $10^{14.5}$, $10^{13}$, and $10^{7.6}$ P, respectively.[4,5] Physically, the strain point represents the temperature below which the glass behaves essentially elastically, the annealing point is the temperature at which internal stresses are relieved within a period of minutes, and the softening point is the temperature at which the glass readily flows at low stresses.

§CMC layers were supplied as unfired fiber–matrix prepregs (Corning).

**Table I. Critical Temperatures for CMC Matrices†**

| Matrix | Strain point (°C) | Annealing point (°C) | Softening point (°C) |
|---|---|---|---|
| Glass (Corning 1723) | ~665 | ~710 | ~910 |
| Glass-ceramic (Corning CAS) | ~1140‡ | ~1245‡ | Not available |

†Data supplied by the manufacturer (Corning, Corning, NY). ‡Apparent value based on beam-bending viscosity of bulk beams.

softening temperatures of the glass and glass-ceramic matrix materials.‡ In one laminate system, the SiC sheets were bonded to the CMC layers by using the glass matrix of the CMC, and, in the other, the SiC sheets were bonded to the CMC layers with the glass-ceramic matrix of the CMC. Fabrication details and room-temperature properties of these laminates have been reported elsewhere.[2]

The delamination resistance, $\Gamma_{ic}$, was measured using edge-notched, four-point flexure tests.[6,7] The laminates were composed of one unidirectional CMC layer that was sandwiched between two ceramic layers (Fig. 1(a)). This geometry was chosen because of its simplicity and because of the need to keep the loading pins in contact with an elastic (nondeforming) medium over the entire range of testing temperatures. Solutions for the delamination strain energy release rate for this three-layer configuration, as well as for the five-layer configuration (Fig. 1(b)), are presented in the Appendix. These solutions were obtained for well-developed delamination cracks for which steady-state conditions apply, as discussed elsewhere.[6,7] Delamination was assumed to occur along or at close proximity to the interface of the outermost ceramic layer with the first fiber-reinforced layer. The homogeneous ceramic layers were considered to be linear elastic and isotropic, with a Young's modulus $E_c$, a Poisson's ratio $\nu_c$, and a thickness $t_c$. On the other hand, the fiber-reinforced layers were considered to be linear elastic and orthotropic, with longitudinal and transverse moduli $E_1^r$ and $E_2^r$ (respectively), in-plane major and minor Poisson's ratios $\nu_{12}^r$ and $\nu_{21}^r$ (respectively), and a thickness $t_r$. This thickness of the fiber-reinforced layers was set equal to $st$, where $s$ is an arbitrary proportionality constant.

As shown in the Appendix and Table A-I, the nondimensional delamination energy release rate is dependent on the bimaterial dissimilarity constant ($\lambda$) and the layer-thickness ratio ($s$) (as given in the Appendix, Eqs. (A-10) and (A-9), respectively). The systems that are under consideration are characterized by a moderate elastic dissimilarity ($\lambda \approx 2.0$). The normalized steady-state energy release rate is plotted against $s$ for various $\lambda$ values in Figs. A-2 and A-3. The calculations indicate that, for the systems that are under consideration, first-ply delamination is more likely to occur in the specimen configuration in which one fiber layer is sandwiched between two ceramic layers (Fig. 1(a)), relative to the configurations that contain a larger number of alternating layers, such as that which is shown in Fig. 1(b). The analysis that is presented in the Appendix neglects residual stresses, because their effects have been shown[3] to be negligible for the systems that are studied herein.

Specimens for testing were cut from larger panels, parallel to the fiber direction. Typical specimen dimensions were ~1.7 mm thick × 3.6 mm wide × 50 mm long. One transverse face which exposed the CMC layer was polished to a 1 μm finish to facilitate observations of damage evolution, as described below. One of the SiC layers was notched using a diamond blade to a depth of ~80% of its thickness (not shown in Fig. 1). Sharp precracks were introduced at the tips of the notches by loading the specimens in three-point bending at room temperature. These cracks did not deflect into the ceramic/CMC interface but did travel across the interface into the CMC layer a short distance (~10–20 μm) and then arrested (Fig. 2). For the subsequent calculations of the energy release rates, the crack depth was considered to be equal to the thickness of the outer SiC layer, which was measured with a micrometer prior to processing.

The precracked specimens were subsequently loaded in four-point flexure, using inner and outer loading spans of 19 and 39 mm, respectively. The tests were performed at temperatures ranging from ambient to 910°C for the glass-matrix composite and to 1350°C for the glass-ceramic-matrix composite. The effects of oxidation embrittlement that occur in Nicalon-containing CMCs[8–11] were precluded by testing in a stagnant argon environment. Prior to testing, the furnace was evacuated to ~$5 \times 10^{-6}$ torr (~$6.7 \times 10^{-4}$ Pa) and subsequently backfilled and flushed with argon three times. The tests were performed in a hydraulic testing machine (Model 810 with a Centorr vacuum furnace, MTS Systems, Eden Prairie, MN). Prior to loading, the specimens were heated at a rate of 10°C/min to the prescribed temperature and held at that temperature for 10 min. The majority of the tests were conducted at a crosshead displacement rate of 0.05 mm/min. Some of the elevated temperature tests were performed at displacement rates of 0.001, 0.08, and 1.0 mm/min.

Damage evolution was monitored in two ways. At room temperature, the polished surfaces were viewed using *in-situ* stereomicroscopy. At high temperatures, it was accomplished by interrupting the tests, cooling the specimens rapidly to ambient temperature (>50°C/min), and examining them via either optical microscopy or scanning electron microscopy (SEM). After examination, the specimens were placed back

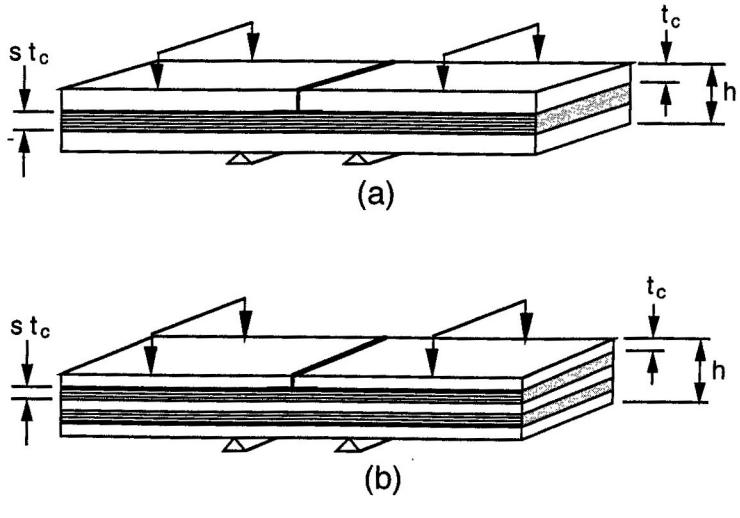


**Fig. 1.** Testing geometries for beams with (a) one fiber layer sandwiched between two dense ceramic layers (SiC for present experiments) and (b) two fiber layers sandwiched between three ceramic layers.

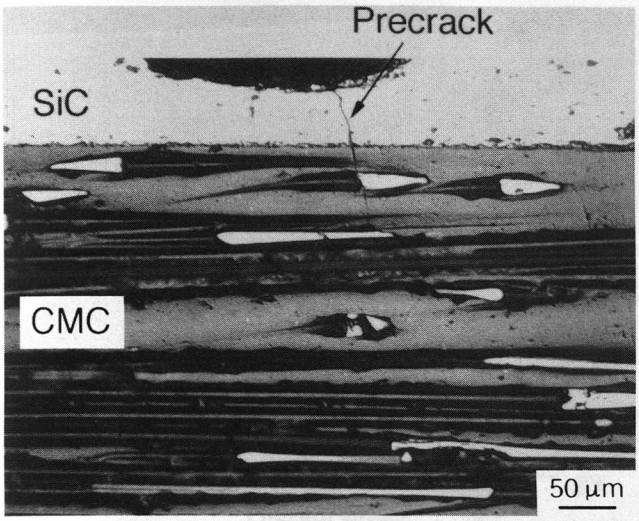


**Fig. 2.** Micrograph of a precrack emanating from a notch and penetrating into the CMC layer.

into the test fixture and loaded to a higher stress level at the same temperature. This procedure was repeated until the experiment was terminated. The tests were terminated when either the load attained a plateau (steady-state) level, independent of displacement, or the load decreased suddenly (the load decreases were associated with the formation of additional cracks in the SiC). There was no difference in the mechanical behavior of the interrupted and uninterrupted tests. Typically one to three tests were performed for each temperature and loading rate. The critical energy release rates that were associated with delamination were obtained from the plateau loads and the solutions for strain energy release rates (see Appendix). In some instances, a plateau stress was not obtained; instead, a second crack formed in the outer SiC layer, which caused a sudden load decrease. When this occurred, the test was terminated; if a delamination crack had formed prior to the load decrease, the peak load was used to calculate a lower-bound estimate of the steady-state delamination resistance. Changes in the Young's modulus of the CMC with temperature were neglected for these calculations.

After testing, the specimens were examined via optical microscopy and SEM. In some instances, the fracture surfaces were exposed by peeling away the top SiC sheet and examined via SEM.

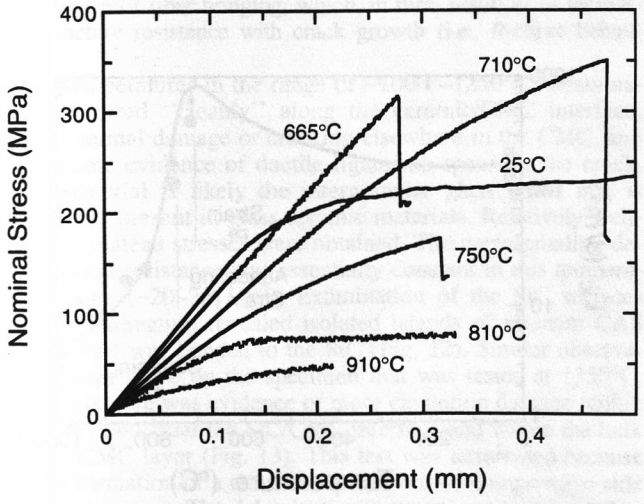


**Fig. 3.** Nominal-stress-versus-displacement curves for SiC/glass-CMC hybrid composites tested at the temperatures noted.

## III. Results and Observations

### *(1) Laminates with Nicalon/1723 Glass CMC*

Figure 3 shows the curves of nominal bending stress versus crosshead displacement for the edge-notched specimens. The curves generally exhibit (i) an initial linear elastic region, (ii) a transient region in which damage occurs ahead of the precrack and the response gradually softens (manifested in a decreasing tangent modulus), and (iii) a plateau (steady-state) stress at which extensive delamination occurs at or near the ceramic/CMC interface. At room temperature, the initial nonlinearity in the stress–displacement response was associated with the formation of matrix cracks that were oriented roughly normal to the interface (Fig. 4(a)). These cracks were typically ~200 μm in length and spaced ~50–100 μm apart. At higher stress levels (approaching the plateau), delamination cracks were observed emanating from the precrack at or near the CMC/ceramic interface. In some instances, the delamination crack followed a somewhat tortuous path through the CMC layer, which resulted in some fiber bridging by inclined fibers (Fig. 4(b)). Similar bridging processes have been observed previously in CMCs under transverse Mode-I loading conditions.[12] However, most of the delamination crack followed a path either along the interface or through the glass matrix near the interface (within ~10 μm). Subsequent examination of the delaminated SiC surfaces revealed remnants of the glass, which was consistent with

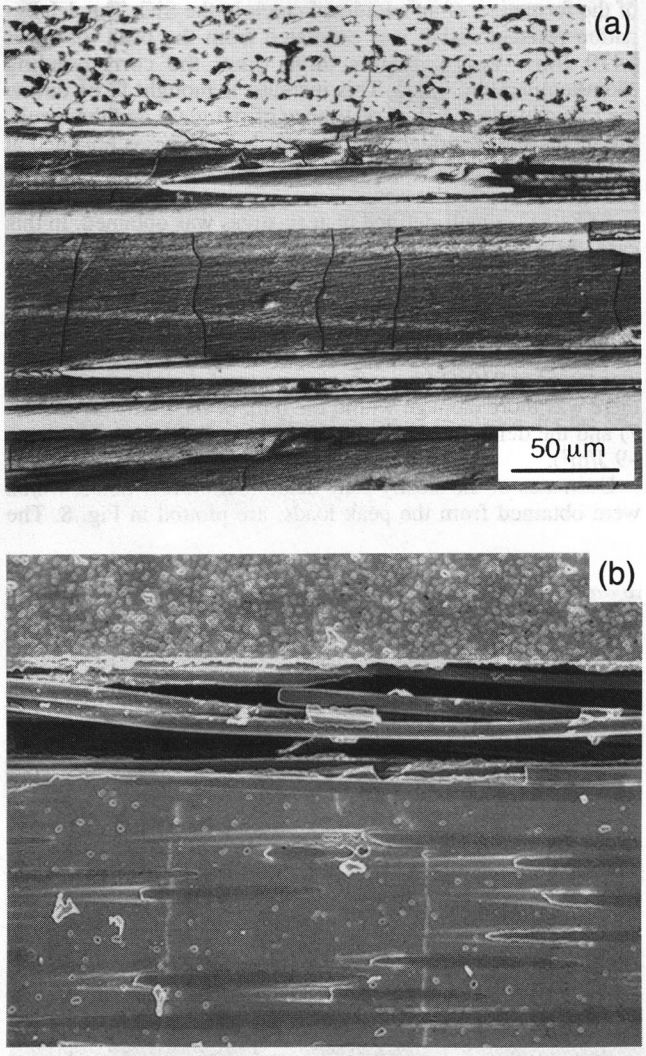


**Fig. 4.** Delamination in the SiC/Nicalon 1723 glass laminate at room temperature, showing (a) accompanying Mode I cracking in the glass matrix and (b) matrix cracking combined with fiber bridging.

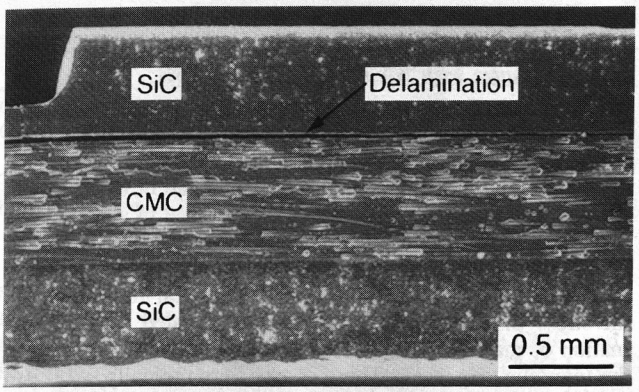


**Fig. 5.** Low-magnification view of delamination at room temperature.

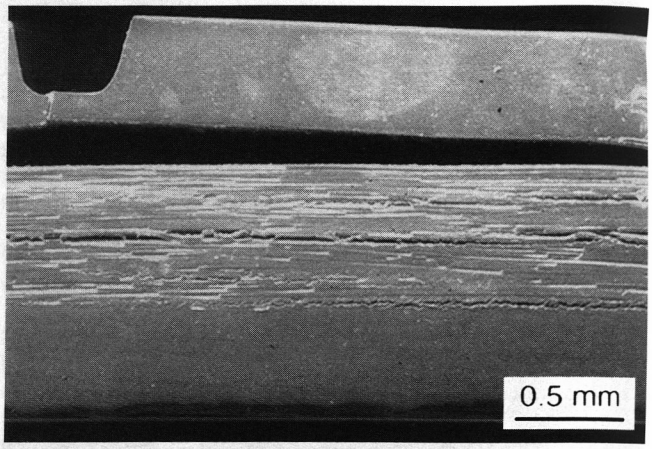


**Fig. 7.** Damage within the bulk of the CMC layer at 865°C.

the observations of the dominant crack propagating partially through the CMC itself rather than along the interface. The delamination resistance was in the range of 140–210 J/m$^2$. These values are only slightly lower than those that were measured using double-cantilever-beam specimens (in Mode I) of the CMC itself (~250 J/m$^2$).[12]

At 710°C (the annealing point of the glass), delamination proceeded in a similar fashion (Fig. 5), although the peak stress was considerably higher and no plateau was obtained, because of the formation of an additional crack in the SiC. The delamination resistance that was estimated from the peak load was ~470 J/m$^2$—approximately three times the corresponding room-temperature value. This increase is thought to be due to the reduction in the flow resistance of the glass and the resulting increase in its toughness. Similar behavior was obtained at 750°C, although delamination and cracking of the SiC both occurred at lower stresses.

At 810°C, a well-defined plateau stress was obtained. In this case, there was no evidence of matrix cracks of the type that are shown in Fig. 4(a). Instead, delamination occurred by a process of cavitation and rupture through the glass matrix very near the ceramic/CMC interface (Fig. 6), with a resistance of only ~20 J/m$^2$. Similar observations were made for the specimen that was tested at 910°C (the softening point of the glass), although there was more damage within the bulk of the CMC layer (Fig. 7) and the delamination resistance was reduced even more (to ~9 J/m$^2$).

Estimates of the steady-state delamination resistance, which were obtained from the peak loads, are plotted in Fig. 8. The data points that are accompanied by arrows indicate that a plateau stress had not been obtained during testing, which suggests that the actual toughness is somewhat higher. Evidently, the interfacial toughness first increases as the temperature increases, up to approximately the annealing point of the glass, but subsequently decreases at higher temperatures, as matrix cavitation becomes the dominant mode of failure.

The effects of the imposed displacement rate (0.001, 0.08, and 1.0 mm/min) on delamination resistance were determined at 865°C, i.e., between the annealing and softening points of the glass matrix. Figure 9 shows the stress–displacement curves and the delamination resistances that have been obtained from these tests. In each of these cases, there was considerable damage in the bulk of the CMC, although failure ultimately occurred at or near the ceramic/CMC interface. The resistance increased approximately an order of magnitude as the displacement rate increased.

### *(2) Laminates with Nicalon–Glass-Ceramic CMC*

Figure 10(a) shows the stress-versus-displacement curves for the laminates that contain the Nicalon–CAS-glass-ceramic CMC. Similar trends were observed in the temperature dependence of the delamination resistance (Fig. 10(b)), although there were some subtle differences in the fracture characteristics. Notably, at low temperatures (<1000°C), delamination proceeded through the CMC itself, at a relatively large distance from the ceramic/CMC interface (~100–300 μm) (Fig. 11). No steady-state toughness was obtained at these temperatures, probably because of the tortuosity of the crack path and the

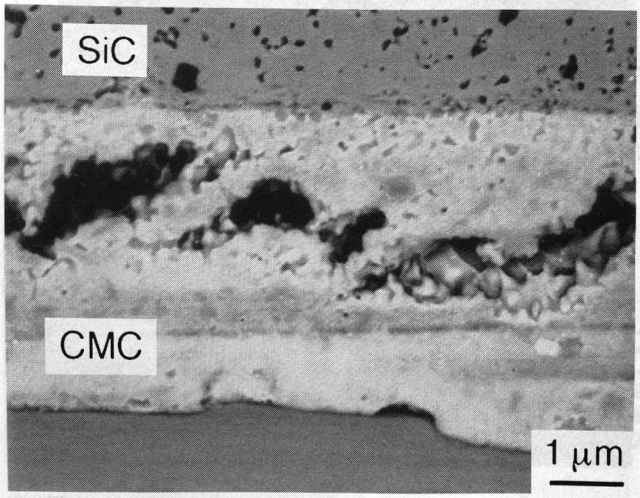


**Fig. 6.** Micrograph of cavitation near the SiC/glass-CMC laminate interface at 810°C.

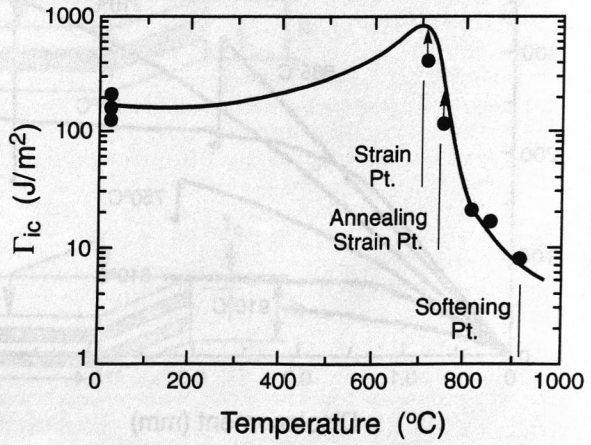


**Fig. 8.** Variation in delamination resistance with temperature for the SiC/glass-CMC system.

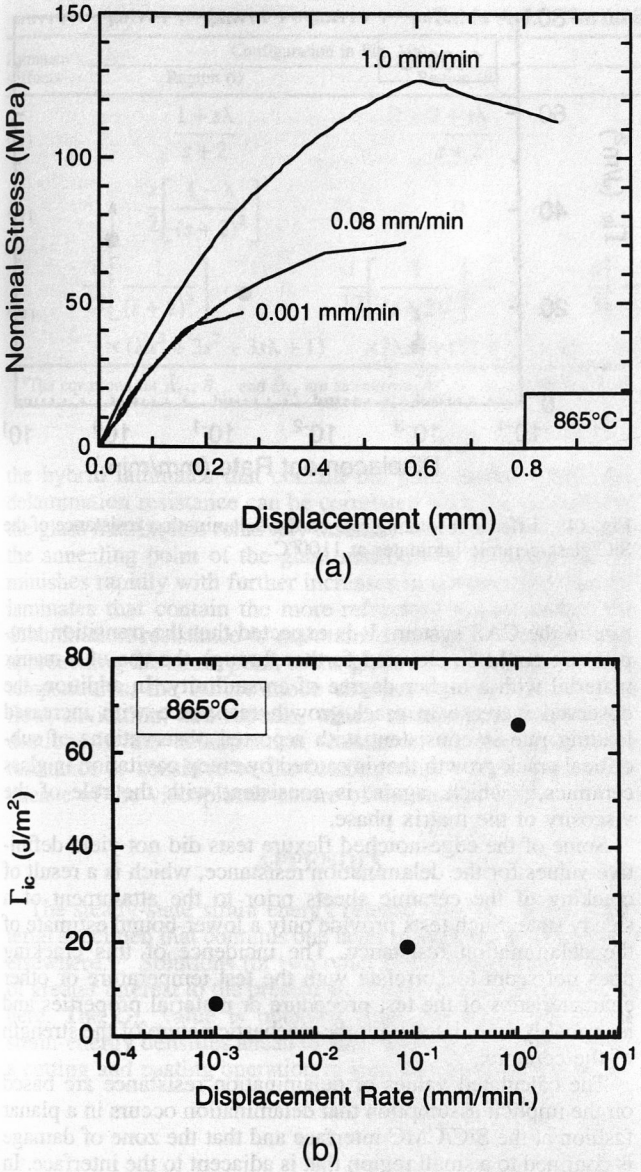


**Fig. 9.** Effects of loading rate on (a) the nominal-stress-versus-displacement curves for the SiC/glass-CMC laminates and (b) the delamination resistance, at 865°C.

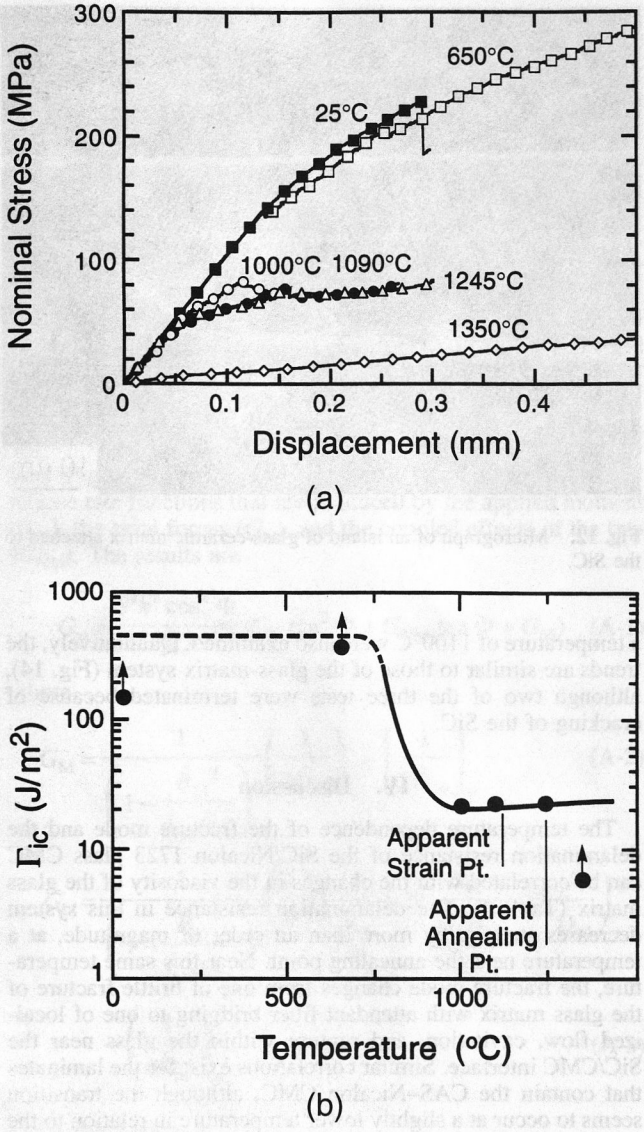


**Fig. 10.** Effects of test temperature on (a) the nominal-stress-versus-displacement curves and (b) the delamination resistance, for the SiC/glass-ceramic laminates.

occurrence of fiber bridging, which, in turn, result in an increasing fracture resistance with crack growth (i.e., *R*-curve behavior).

At temperatures in the range of ~1000°–1250°C, delamination occurred ''cleanly'' along the ceramic/CMC interface, with minimal damage or cracking elsewhere in the CMC, and with some evidence of ductile ligaments spanning the crack. This material is likely the intergranular glass phase that is invariably present in glass-ceramic materials. Relatively well-defined plateau stresses were obtained. The corresponding delamination resistance was essentially constant in this temperature range (~20–25 J/m$^2$). Examination of the SiC surfaces after delamination revealed isolated islands of remnant CAS matrix that was bonded to the SiC (Fig. 12). Similar observations were made on the specimen that was tested at 1350°C, although there was evidence of more cavitation damage within the CAS both near the SiC/CMC interface and within the bulk of the CMC layer (Fig. 13). This test was terminated because of the formation of a crack in the SiC on the compressive side of the specimen. The delamination resistance was estimated to be greater than ~6 J/m$^2$.

The effects of loading rate on the delamination resistance at

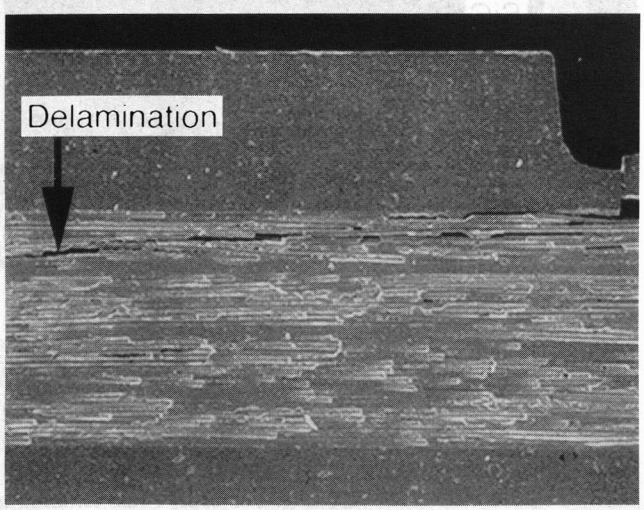


**Fig. 11.** Delamination in the SiC/glass-ceramic CMC at 650°C.

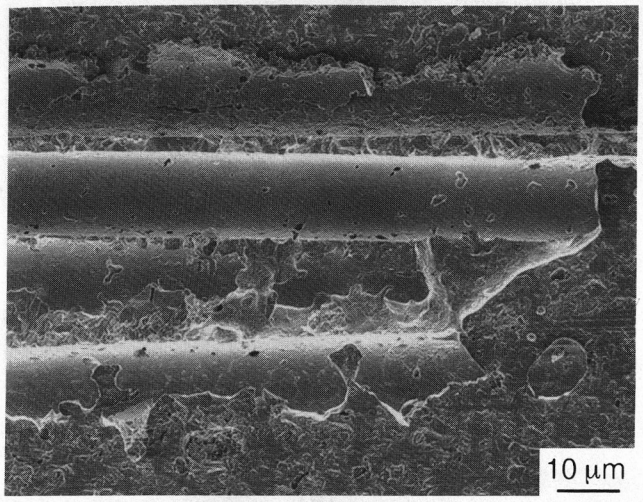


**Fig. 12.** Micrograph of an island of glass-ceramic matrix attached to the SiC.

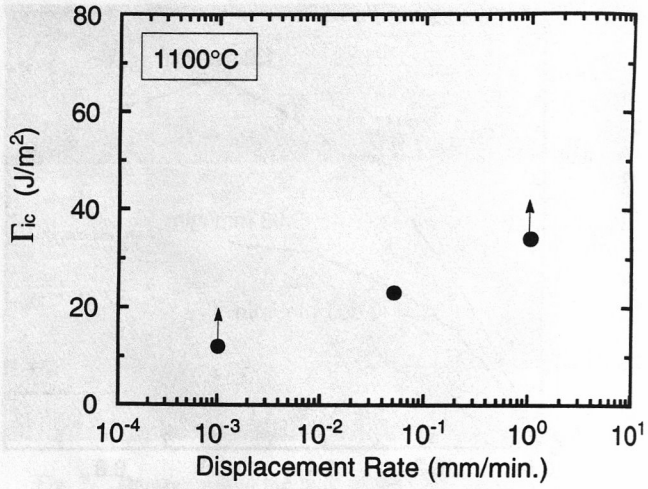


**Fig. 14.** Effects of loading rate on the delamination resistance of the SiC/glass-ceramic laminates at 1100°C.

a temperature of 1100°C were also examined. Qualitatively, the trends are similar to those of the glass-matrix system (Fig. 14), although two of the three tests were terminated because of cracking of the SiC.

## IV. Discussion

The temperature dependence of the fracture mode and the delamination resistance of the SiC/Nicalon 1723 glass CMC can be correlated with the changes in the viscosity of the glass matrix (Table I). The delamination resistance in this system decreases steeply, by more than an order of magnitude, at a temperature near the annealing point. Near this same temperature, the fracture mode changes from one of brittle fracture of the glass matrix with attendant fiber bridging to one of localized flow, cavitation, and rupture within the glass near the SiC/CMC interface. Similar correlations exist for the laminates that contain the CAS–Nicalon CMC, although the transition seems to occur at a slightly lower temperature in relation to the strain point of the CAS. (The absolute temperature of the transition in the CAS laminate is higher, because of the more-refractory nature of the glass-ceramic.) These materials contain some residual glassy phase at the grain boundaries, which seems to control the fracture resistance at higher temperatures; this is believed to be the cause of the lower transition temperature in the CAS system. It is expected that the transition temperature could be elevated further through the use of a matrix material with a higher degree of crystallinity. In addition, the observed increase in crack-growth resistance with increased loading rate is consistent with reported observations of subcritical crack growth that is caused by creep cavitation in glass ceramics,[13] which, again, is consistent with the role of the viscosity of the matrix phase.

Some of the edge-notched flexure tests did not yield definitive values for the delamination resistance, which is a result of cracking of the ceramic sheets prior to the attainment of a steady state. Such tests provide only a lower-bound estimate of the delamination resistance. The incidence of this cracking does not seem to correlate with the test temperature or other characteristics of the test procedure or material properties and is probably associated with the stochastic nature of the strength of the ceramic.

The calculated values of delamination resistance are based on the implicit assumption that delamination occurs in a planar fashion at the SiC/CMC interface and that the zone of damage is confined to a small region that is adjacent to the interface. In some instances, the zone of microcracks extends ~200 μm into the CMC; in others, the delamination crack deviates gradually from the plane of the interface, by as much as ~300 μm. These effects may become important when the corresponding lengths become comparable to the layer thickness (~0.5–1 mm in the present experiments). The magnitude of those effects can be probed experimentally by measuring the delamination resistance in thicker test specimens.

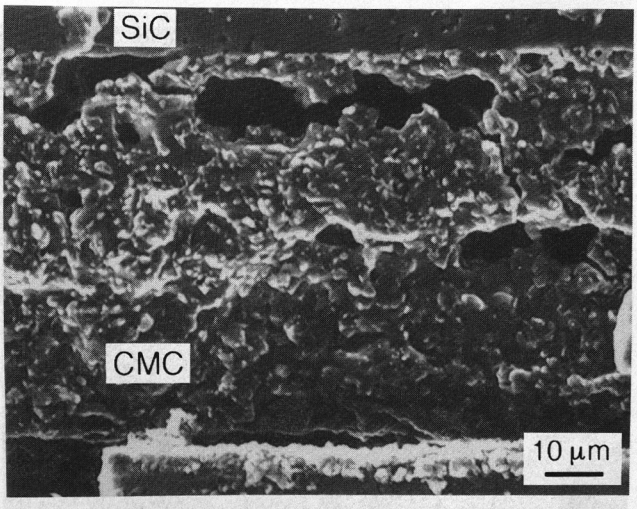


**Fig. 13.** Cavitation in the SiC/glass-ceramic-CMC laminate near the SiC/CMC interface at 1350°C.

## V. Conclusions

The delamination resistance of the hybrid laminates is sensitive to the matrix phase within the CMC, because this is the bonding agent between the ceramic and the CMC layers. For

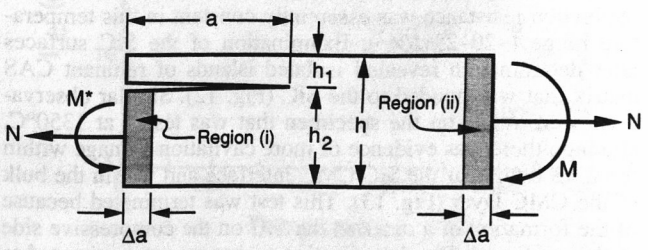


**Fig. A-1.** Schematic of a symmetric half of delaminated composite beam subjected to combined axial loading and bending.

**Table A-I. Normalized Laminate Stiffnesses**

| Laminate stiffness† | Configuration in Fig. 1(a) | | Configuration in Fig. 1(b) | |
|---|---|---|---|---|
| | Region (i) | Region (ii) | Region (i) | Region (ii) |
| $\hat{A}_{11}$ | $\frac{1+s\lambda}{s+2}$ | $\frac{2+s\lambda}{s+2}$ | $\frac{2(1+s\lambda)}{3+2s}$ | $\frac{3+2s\lambda}{3+2s}$ |
| $\hat{B}_{11}$ | $\frac{s}{2}\left[\frac{1-\lambda}{(s+2)^2}\right]$ | 0 | $\frac{s(1-\lambda)}{(3+2s)^2}$ | 0 |
| $\hat{D}_{11}$ | $\frac{1}{12}\left[\frac{1}{(s+2)^3}\right]$ $\times(\lambda s^3+3s^2+3s\lambda+1)$ | $\frac{1}{12}\left[\frac{1}{(s+2)^3}\right]$ $\times[\lambda s^3+6(1+s)^2+2]$ | $\frac{1}{3}\left[\frac{1}{(3+2s)^3}\right]$ $\times[3s(1+\lambda)(1+s)+2(1+s^3\lambda)]$ | $\frac{1}{12}\left[\frac{1}{(3+2s)^3}\right]$ $\times[8\lambda s^3+12s^2(2+\lambda)+6s(8+\lambda)+27]$ |

†The equations for $\hat{A}_{11}$, $\hat{B}_{11}$, and $\hat{D}_{11}$ are as follows: $\hat{A}_{11} = A_{11}/(Q_c h)$, $\hat{B}_{11} = B_{11}/(Q_c h^2)$, and $\hat{D}_{11} = D_{11}/(Q_c h^3)$, where $Q_c = E_c/(1-\nu_c^2)$.

the hybrid laminates that contain the glass-matrix CMC, the delamination resistance can be correlated with the viscosity of the glass matrix; it is relatively insensitive to temperature, up to the annealing point of the glass matrix, and subsequently diminishes rapidly with further increases in temperature. For the laminates that contain the more-refractory glass-ceramic, the delamination resistance is maintained to higher temperatures, approaching the strain point of the glass-ceramic. Beyond these temperatures, the failure mode changes to one that involves flow, cavitation, and rupture, which results in substantial reductions in the delamination resistance. In this regime, the resistance is sensitive to the loading rate, which is a consequence of the viscoplastic nature of the matrix phase.

## APPENDIX

The steady-state strain energy release rate, $G_{ss}$, for a bimaterial specimen that contains one layer of each material is found elsewhere.[3,7] Solutions for two other beam geometries that are of greater interest to the present work (see Fig. 1) are presented here. The $G_{ss}$ value is obtained from the difference in the strain-energy densities ahead of and behind the crack tip, using a cutting and pasting operation to simulate virtual crack extension (Fig. A-1). It is expressed as the sum of the strain energy release rate functions that are produced by the applied moment ($G_M$), the axial forces ($G_N$), and the coupled effects of the two ($G_{NM}$). The results are

$$G_{ss} = \frac{S^2 h^2 \cos^2 \Phi}{3\bar{D}} (G_N \tan^2 \Phi + G_{NM} \tan \Phi + G_M) \quad \text{(A-1)}$$

where

$$G_M = \frac{1}{\left(1 - \frac{\hat{B}_{11}^2}{\hat{A}_{11}\hat{D}_{11}}\right)_i} \left(\frac{1}{8\hat{D}_{11}}\right)_i - \left[\frac{1}{8\hat{D}_{11}}\right]_{ii} \quad \text{(A-2)}$$

$$G_N = \frac{1}{\left(1 - \frac{\hat{B}_{11}^2}{\hat{A}_{11}\hat{D}_{11}}\right)_i} \left(\frac{1}{8}\right)\left(\frac{1}{\hat{A}_{11}} + 2\bar{y}\frac{\hat{B}_{11}}{\hat{A}_{11}\hat{D}_{11}} + \bar{y}^2\frac{1}{\hat{D}_{11}}\right)_i - \left(\frac{1}{8\hat{A}_{11}}\right)_{ii} \quad \text{(A-3)}$$

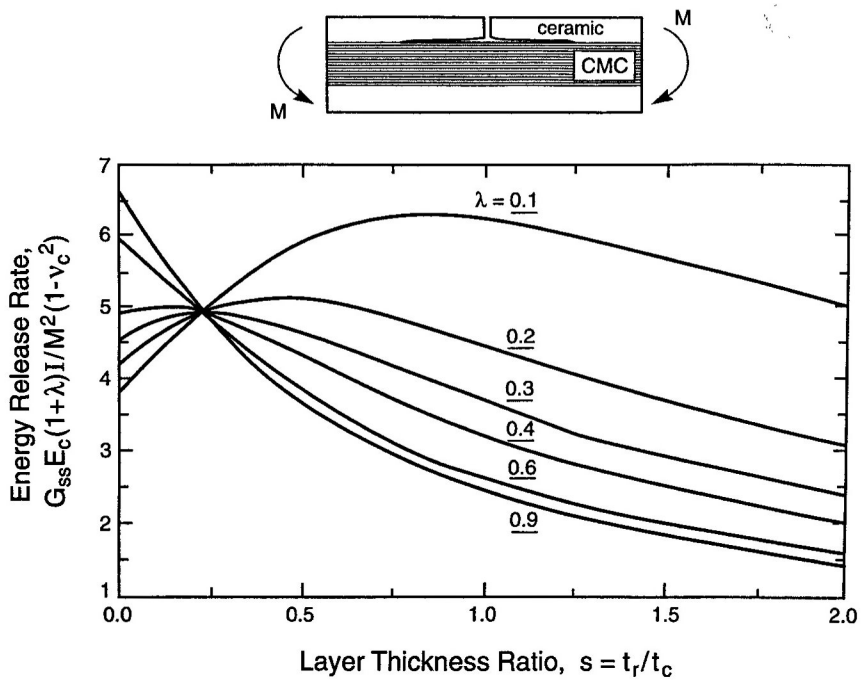


**Fig. A-2.** Variation in the normalized energy release rate, $\hat{G}$, with the layer-thickness ratio $s$ (equal to $t_f/t_c$) and the elastic dissimilarity constant, $\lambda$, in the range of 0.1–0.9. Results were obtained assuming delamination of the top ply in a three-layer composite, as shown in the schematic above the graph.

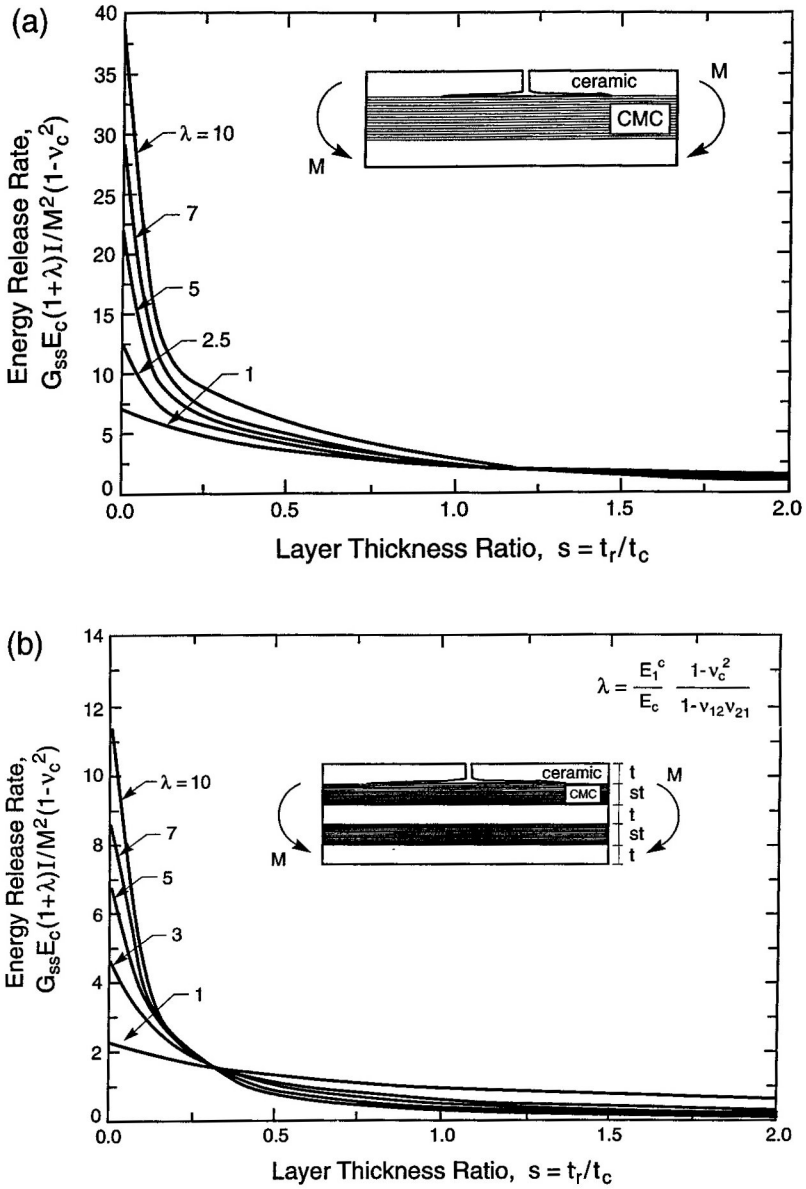


**Fig. A-3.** Variation in the normalized energy release rate, $\hat{G}$, with the layer-thickness ratio $s$ (equal to $t_r/t_c$) for (a) a three-layer composite and (b) a five-layer composite. Results were obtained using elastic dissimilarity constant, λ, values in the range of 1.0–10.0.

$$G_{NM} = \frac{1}{\left(1 - \frac{\hat{B}_{11}^2}{\hat{A}_{11}\hat{D}_{11}}\right)_i}\left(\frac{1}{4}\right)\left(\frac{\hat{B}_{11}}{\hat{A}_{11}\hat{D}_{11}} + \bar{y}\frac{1}{\hat{D}_{11}}\right)_i \quad \text{(A-4)}$$

$$\bar{y} = \frac{\xi}{2(1+\xi)} \quad \text{(A-5)}$$

$$\overline{D} = \left(\frac{E_c}{1-\nu_c^2}\right)\frac{h^2}{12} \quad \text{(A-6)}$$

$$S = \frac{M}{h\cos\Phi} = \frac{Pl}{2bh\cos\Phi} \quad \text{(A-7)}$$

$$\xi = \frac{h_1}{h_2} \quad \text{(A-8)}$$

$$s = \frac{t_r}{t_c} \quad \text{(A-9)}$$

$$\lambda = \frac{E_1^r}{E_c}\left(\frac{1-\nu_c^2}{1-\nu_{12}^r\nu_{21}^r}\right) \quad \text{(A-10)}$$

$$\tan\Phi = \frac{Nh}{M} \quad \text{(A-11)}$$

Here, $E_c$ and $\nu_c$ are the Young's modulus and Poisson's ratio, respectively, of the precracked (ceramic) layer; $P$ is the plateau load, $l$ the distance between the inner and outer loading points, $b$ the specimen width, and $h$ the specimen height. The thickness of the uncracked and cracked layers are, respectively, $h_1$ and $h_2$, and $t_c$ and $t_r$ are the thickness of the ceramic and CMC-reinforced layers, respectively. $M$ is the applied moment, and $N$ is the applied normal force; the normalized stiffnesses—$\hat{A}_{11}$, $\hat{B}_{11}$, and $\hat{D}_{11}$—for the two regions that are illustrated in Fig. A-1 are found in Table A-I. Some typical results are plotted in Figs. A-2 and A-3.

## References

[1]C. A. Folsom, F. W. Zok, F. F. Lange, and D. B. Marshall, "Mechanical Behavior of a Laminar Ceramic/Fiber-Reinforced Epoxy Composite," *J. Am. Ceram. Soc.*, **75** [11] 2969–75 (1992).

[2]W. A. Cutler, F. W. Zok, and F. F. Lange, "Mechanical Behavior of Several Hybrid CMC Laminates," *J. Am. Ceram. Soc.*, **79** [7] 1825–33 (1996).

[3]W. A. Cutler, "Processing and Mechanical Behavior of High Temperature Hybrid Laminated Composites"; Ph.D. Dissertation. University of California. Santa Barbara, CA, 1995.

[4](a)"Standard Test Method for Softening Point of Glass," ASTM Designation C 338–93. *1996 Annual Book of ASTM Standards,* Vol. 15.02, pp. 100–102. American Society for Testing and Materials, Philadelphia, PA. (b) "Standard Test Method for Annealing Point and Strain Point of Glass by Beam Bending," ASTM Designation C 598–93. *ibid,* pp. 154–58.

[5]D. C. Boyd and D. A. Thompson, "Glass," *Kirk–Othmer: Encycl. Chem. Technol., 3rd Ed.,* **11** [3] 807–80 (1980).

[6]P. G. Charalambides, H. C. Cao, J. Lund, and A. G. Evans, "Development of a Test Method for Measuring the Mixed Mode Fracture Resistance of Bimaterial Interfaces," *Mech. Mater.*, **8**, 269–83 (1990).

[7]P. G. Charalambides, J. Lund, A. G. Evans, and R. M. McMeeking, "A Test Specimen for Determining the Fracture Resistance of Bimaterial Interfaces," *J. Appl. Mech.*, **56**, 77–82 (1989).

[8]T. Mah, M. G. Mendiratta, A. P. Katz, R. Ruh, and K. S. Mazdiyasni, "High-Temperature Mechanical Behavior of Fiber-Reinforced Glass-Ceramic-Matrix Composites," *J. Am. Ceram. Soc.*, **68** [9] C-248–C-251 (1985).

[9]J. J. Brennan, "Interfacial Characterization of Glass and Glass-Ceramic Matrix/Nicalon SiC Fiber Composites," *Mater. Sci. Res.*, **20**, 546–60 (1986).

[10]L. Filipuzzi, G. Camus, R. Naslain, and J. Thebault, "Oxidation Mechanisms and Kinetics of 1D-SiC/C/SiC Composite Materials: I, An Experimental Approach," *J. Am. Ceram. Soc.*, **77** [2] 459–66 (1994).

[11]F. E. Heredia, J. C. McNulty, F. W. Zok and A. G. Evans, "Oxidation Embrittlement Probe for Ceramic-Matrix Composites," *J. Am. Ceram. Soc.*, **78** [8] 2097–100 (1995).

[12]S. M. Spearing and A. G. Evans, "The Role of Fiber Bridging in the Delamination Resistance of Fiber-Reinforced Composites," *Acta Metall. Mater.*, **40** [9] 2191–99 (1992).

[13]K. S. Chan and R. A. Page, "Origin of the Creep-Crack Growth Threshold in a Glass-Ceramic," *J. Am. Ceram. Soc.*, **75** [3] 603–12 (1992). □